Control of the diocotron instability of a hollow electron beam with periodic dipole magnets

Y. H. Jo, J. S. Kim, G. Stancari, M. Chung, and H. J. Lee

Citation: Physics of Plasmas **25**, 011607 (2018);
View online: https://doi.org/10.1063/1.5018425
View Table of Contents: http://aip.scitation.org/toc/php/25/1
Published by the American Institute of Physics

Control of the diocotron instability of a hollow electron beam with periodic dipole magnets

Y. H. Jo,[1] J. S. Kim, G. Stancari,[2] M. Chung,[3,a)] and H. J. Lee[1,b)]
[1]*Department of Electrical Engineering, Pusan National University, Busan 609–735, South Korea*
[2]*Fermi National Accelerator Laboratory, P.O. Box 500, Batavia, Illinois 60510, USA*
[3]*Department of Physics, Ulsan National Institute of Science and Technology, Ulsan 689–798, South Korea*

(Received 31 March 2017; accepted 25 May 2017; published online 28 December 2017)

A method to control the diocotron instability of a hollow electron beam with periodic dipole magnetic fields has been investigated by a two-dimensional particle-in-cell simulation. At first, relations between the diocotron instability and several physical parameters such as the electron number density, the current and shape of the electron beam, and the solenoidal field strength are theoretically analyzed without periodic dipole magnetic fields. Then, we study the effects of the periodic dipole magnetic fields on the diocotron instability using the two-dimensional particle-in-cell simulation. In the simulation, we considered the periodic dipole magnetic field applied along the propagation direction of the beam, as a temporally varying magnetic field in the beam frame. A stabilizing effect is observed when the oscillating frequency of the dipole magnetic field is optimally chosen, which increases with the increasing amplitude of the dipole magnetic field. *Published by AIP Publishing.* https://doi.org/10.1063/1.5018425

I. INTRODUCTION

In the research field of non-neutral plasma physics, the active control of a diocotron instability remains as an important and practical research issue. The diocotron instability is one of the common plasma instabilities induced by the same underlying mechanism as the Kelvin-Helmholtz instability, which is evolved by a shear in the flow velocity of surface waves.[1–7] Typically, the diocotron instabilities are observed during the propagation of non-neutral hollow electron beams (or annular electron layers) along a drift section.

Recently, a novel beam collimation concept based on the hollow electron beam has been proposed in the high-energy particle accelerator community.[8–11] In the proposed collimator system, as shown in Fig. 1, a hollow electron beam encloses a circulating beam (e.g., a proton beam for the Large Hadron Collider at CERN) and induces radial nonlinear space-charge kicks only to the high-amplitude halo particles. The overlap region is typically a few meters, and for this study, the specific propagation length of 2.51 m was chosen. If the hollow electron beam remains stable and perfectly symmetric, it would drive the halo particles toward the collimators in a controlled manner without disturbing the core of the circulating beam as desired. On the other hand, if the hollow electron beam becomes distorted by the diocotron instability, it would produce finite electric or magnetic fields inside and eventually perturb the beam core. Hence, it is of great importance to choose operating parameters (e.g., electron beam density, beam sizes, and magnetic field strength) properly so that the growth of the instability is minimized. If there are certain limitations for the choices of the parameters, however, we should find other active means of controlling the diocotron instability. In this study, we focus on the control of the diocotron instability by applying periodic dipole magnetic field components.

For simplicity, we consider the hollow electron beam only without the circulating beam inside. The propagation length of the hollow electron beam in Fig. 1 is 2.51 m, which will be used as the characteristic axial length L of the system in this study. The transit time of the beam is defined as the time for the electron beam to pass through the propagation length once. The assumption of the low density electron $\omega_{pe} \ll \omega_{ce}$ is used for the electrostatic perturbation in the present analyses, where ω_{pe} is the electron plasma frequency and ω_{ce} is the electron cyclotron frequency. More details of the simulations will be presented in the following sections.

Analytical investigations on the diocotron instability are introduced in Secs. II and III based on some of our previous works.[12–16] Although they are obtained with approximations, the analytical expressions explain the relationship among several important physical parameters which could directly affect the diocotron instability. Most of those parameters are considered as control variables in the simulation study. As an active means of suppressing the diocotron instability, a periodic dipole magnetic field is introduced in Sec. IV. In Sec. V, the effects of periodic dipole magnetic fields on the diocotron instability are presented with the numerical results obtained by two-dimensional particle-in-cell (PIC) simulations. Finally, the conclusion of this study is given in Sec. VI.

II. STABILITY ANALYSIS

The governing equation for the perturbed electrostatic potential ϕ of a uniform hollow electron beam in the cylindrical geometry is[14]

$$\left(\frac{\partial}{\partial t}+\Omega(r)\frac{\partial}{\partial \theta}\right)\nabla^2\phi(r,\theta,t)=2\Omega_D\frac{\partial\phi}{\partial\theta}\frac{1}{r}\frac{dn_{e0}}{dr}, \qquad (1)$$

a)Electronic mail: mchung@unist.ac.kr
b)Electronic mail: haejune@pusan.ac.kr

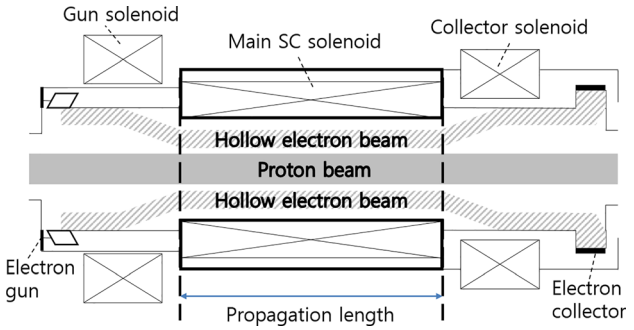

FIG. 1. Conceptual layout of the collimator system.[9,10]

where the diocotron frequency Ω_D is

$$\Omega_D = \frac{\omega_{pe}^2}{2\omega_{ce}} \propto \frac{n_{e0}}{B}, \tag{2}$$

and the angular velocity $\Omega(r)$ is equal to

$$\Omega(r) = \Omega_D\left(1 - \frac{b^2}{r^2}\right), \tag{3}$$

in $b \le r \le d$. Here, n_{e0} is the electron density and b and d are the inner and the outer radii of the electron beam, respectively. This governing equation is derived based on the drift-Poisson model of the low-density cylindrical annular plasma column confined by a uniform magnetic field **B** applied in the axial direction of the column. With the Fourier transform in the θ coordinate, an analytical solution for ϕ was obtained in Ref. 14, which allows us to get an expression for the growth rate of the electrostatic perturbation of the hollow electron beam in the cylindrical geometry with the conducting boundary as

$$\gamma(l) = \frac{\Omega_D}{2}\left\{4\frac{b^{2l}}{d^{2l}}\left[1 - l\left(1 - \frac{b^2}{d^2}\right)\frac{d^{2l}}{R^{2l}}\right] - \left[2 - l\left(1 - \frac{b^2}{d^2}\right) - \frac{d^{2l}}{R^{2l}}\left(1 - \frac{b^{2l}}{d^{2l}}\right)\right]^2\right\}^{1/2}, \tag{4}$$

for the azimuthal mode number l. Here, R is the radius of the conducting boundary. The result indicates that the cylindrical diocotron instability is observed for $l \ge 2$ because the growth rate has a non-zero value for such conditions. We note that both the growth rate and the dominant mode number become bigger as the beam becomes thinner as shown in Fig. 2. Also, it is obvious that the growth rate is proportion to the diocotron frequency, which means that the instability grows in proportion to n_{e0}/B when the parameters associated with the beam thickness are fixed.

A radially uniform beam profile was assumed in the theory, which causes the stable $l = 1$ mode. However, the realistic experimental beam profile is not radially uniform, and it was reported that the $l = 1$ mode becomes unstable in an inhomogeneous electron column with a stationary point in the non-monotonic equilibrium rotation frequency profile.[13] In spite of valuable theoretical efforts, the $l = 1$ mode was not observed in the conventional modal analysis.[17] However, the inclusion of a radially inhomogeneous density profile in a nonmodal initial value problem is not considered in this study.

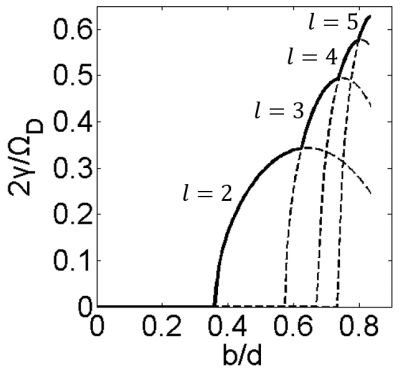

FIG. 2. Plots of the normalized growth rate of the unstable modes versus the relative thickness, b/d, of the annular cylindrical beam for azimuthal numbers $l = 2, 3, 4, 5$ with fixed $d/R = 0.8$.

III. BEAM PROFILE EVOLUTION

In this section, a method to predict the beam profile after propagation through the characteristic axial length of the collimator system is presented. For the analysis, we consider a uniform low-density electron column confined in an axially applied magnetic field. The realistic three-dimensional beam dynamics was analyzed using a two-dimensional simulation without considering the beam front effect, which is a transient phenomenon. It was assumed that the z-dimensional wavelength is quite large. That is to say, $k_z L \ll 1$, where k_z is the wavenumber in the axial direction. With this condition, the radial equilibrium electric field induces a slow rotation of the column through $\mathbf{E} \times B$ drift. The angular rotation frequency is approximately given by the diocotron frequency Ω_D. The total rotation phase φ of the electron column during the transit time $\Delta T \approx L/v_z$ can be expressed as

$$\varphi \approx \Omega_D \Delta T \propto \frac{n_{e0}}{B}\frac{L}{v_z}, \tag{5}$$

where L is the characteristic axial length of the system and v_z is the axial velocity of the electron beam which is assumed to be constant. If the electrons emitted from the cathode behave as the non-relativistic Child-Langmuir flow, the current density is

$$J = n_{e0} e v_z \propto V^{3/2}, \tag{6}$$

where V is the cathode voltage and $v_z \approx (2eV/m_e)^{1/2} \propto V^{1/2}$. Combining Eqs. (5) and (6), we find that the rotation phase of the electron column is determined by

$$\varphi \approx const. \times \frac{\sqrt{V}}{B} L. \tag{7}$$

Since the evolution of the beam cross-section depends on the rotation phase φ, we expect that the shapes of the transverse beam profiles measured at the axial distance L would be more or less similar for the same values of $\sqrt{V}/B$. In other words, we may use the single scaling parameter $\sqrt{V}/B$ to predict the beam profile. Even though this scaling is obtained for the uniform electron beam, it could be applied for the hollow beam as well, provided that the width of the hollow beam is small compared with its inner radius.

IV. PERIODIC DIPOLE MAGNETIC FIELD

From the theoretical analyses above, we may conclude that there are enough parameter knobs we can adjust for the control of the diocotron instability. Although less density, thicker electron beam layer, and higher magnetic field strength are helpful for stabilizing the diocotron instability, there are certain limits for each parameter. For the proton beam collimation, the electron beam density should be above a certain level so that it can maintain the effect of "kicking" the halo particles around the proton beam. The thick electron beam layer and high magnetic field strength could increase the cost of the experimental apparatus significantly. Therefore, we need to investigate an alternative way to control the diocotron instability of the hollow electron beam. Motivated by periodic magnetic focusing of sheet electron beams,[18] we consider periodic dipole magnetic fields to suppress the diocotron instability. The field configuration with periodic dipole magnetic fields added to a solenoidal field can be represented by

$$\mathbf{B}(z) = B_u \cos\phi(z)\hat{x} + B_z\hat{z}. \tag{8}$$

The oscillating phase $\phi(z)$ of the magnetic field is related to the propagation time $t = z/v_z$ as

$$\phi = \phi_0 + 2\pi f_u t. \tag{9}$$

If the dipole magnetic fields make m_ϕ oscillations during the transit time ΔT, one obtains the temporal frequency $f_u = m_\phi/\Delta T$. In terms of the spatial variables, one can have the periodicity of the dipole $\lambda = L/m_\phi$. The actual implementation of the periodic dipole magnetic field is straightforward and technically feasible. The details of the effects of the periodic dipole magnetic fields will be discussed in Sec. V.

V. SIMULATION RESULTS

A. Validation of simulation

A two-dimensional cylindrical particle-in-cell simulation was performed to investigate the effects of the periodic dipole magnetic field applied to the electron beam. The simulation code was modified from the XPDC2 code originally developed at the Plasma Theory and Simulation Group in the University of California at Berkeley.[19]

The simulation domain and the initial density profile are shown in Fig. 3. Since the initial transverse velocities of electrons are set to zero and the initial electron temperature T_{e0} is about 2.85×10^{-4} eV, it can be considered that electrons do not have a transverse velocity distribution. The reason that most of the electrons are distributed at the inner side of the hollow beam is to maximize the effect of "kicking" halo particles of the proton beam.[9] This non-uniformity of the density makes the analytical calculation of the diocotron frequency Ω_D rather difficult, so we will not use it explicitly in this section. The cylindrical conductor of a radius $R = 3$ cm is assumed to be grounded. The values of the beam radii b and d are chosen based on the shape of the hollow cathode electron gun used in the experimental setup. The

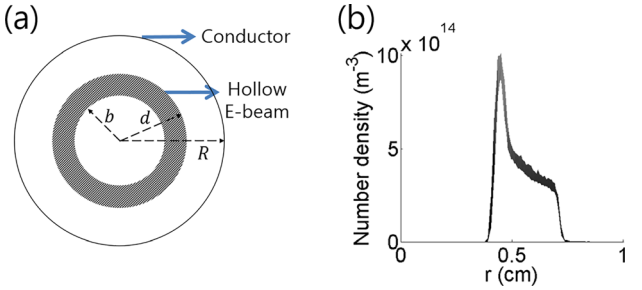

FIG. 3. (a) The simulation domain of a hollow electron beam in the cylindrical geometry and (b) initial density profile from the experiment.

outer diameter of the beam is $2d = 1.524$ cm, and the inner diameter is $2b = 0.8$ cm.

Figure 4 shows the modification of the density profiles of the hollow electron beam by the diocotron instability for the variations of peak densities and magnetic field strengths. The cathode voltage is set to 9 kV for this case, which yields that the axial velocity of the electron beam is $v_z = 5.622 \times 10^7$ m/s. The theoretical analysis made in Sec. II for the annular electron column with a uniform density profile indicates that the growth rate of the diocotron instability is proportion to n/B. In the previous work,[14] it was reported that the theory is in good agreement with the numerical simulation for a uniform beam case. Figure 4 illustrates the same patterns for each column which has the same n/B. It means that the theoretical estimation is still valid even for non-uniform density cases. Qualitatively, the dominant azimuthal mode number is six for these cases.

Figure 5(a) shows the density profiles of the hollow electron beam after propagating for a transit time ΔT. For the comparisons of the analytic results in Sec. III with the simulation results, a hollow electron beam with a uniform density profile is launched for the results in Fig. 5. Three lines (1)–(3) indicate the cases with three different scaling parameters, $(V[\mathrm{kV}])^{1/2}(B[\mathrm{T}])^{-1} = 5$, 10, and 15, respectively. It appears that the beam cross-sectional shapes are very similar for the same values of $\sqrt{V}/B$. For numerical verifications, the normalized Fourier-transformed electrostatic potentials for each case are shown in Fig. 5(b). Here, the normalization factor ϕ_{k0} is measured from the uniform initial profiles. The lines are connecting the average values of ϕ_k/ϕ_{k0} for a given $\sqrt{V}/B$ value, and the error bars indicate the standard deviations. It is clear that the mode structures have the same tendency when they have the same scaling parameters $\sqrt{V}/B$. The dominant mode number is four for each case, and the mode structures are more clearly observed for larger values of $\sqrt{V}/B$ as shown in line (3).

The same numerical investigation was performed for the cases of non-uniform initial densities (see Fig. 6). The initial density profiles applied for the simulations were chosen as close as possible to the experimental measurements.[20] It is clear that the mode structures for these cases also have the same tendency when they have the same scaling parameter $\sqrt{V}/B$. Even though the dominant mode does not clearly appear because of the noise from spatial distribution, the overall tendency is apparently the same with the

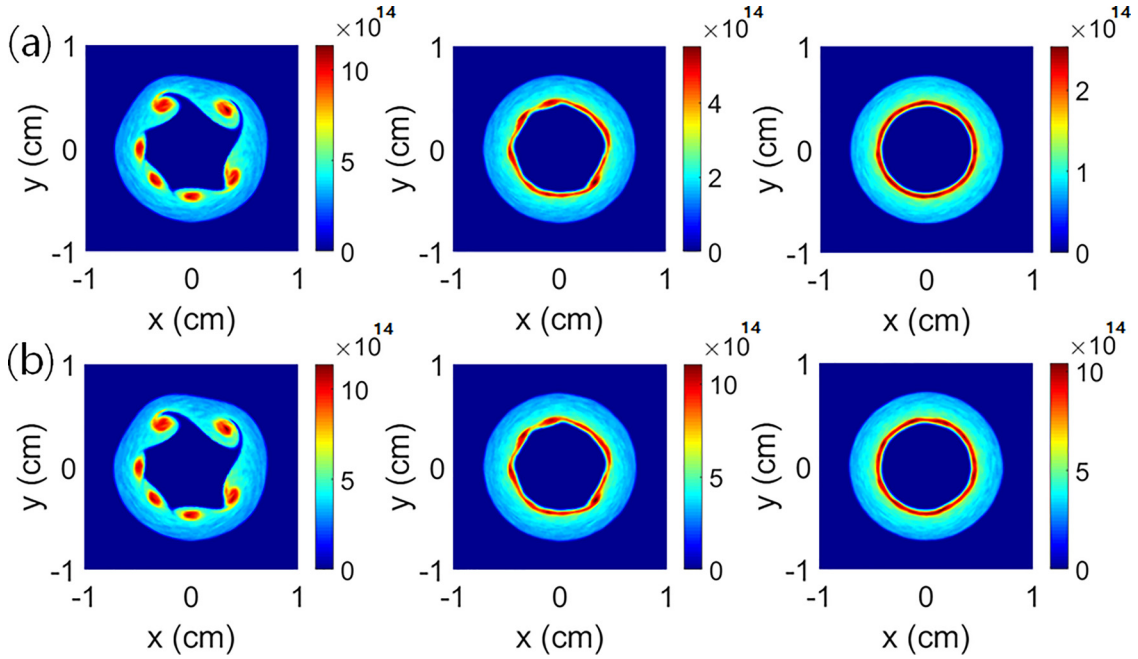

FIG. 4. Two-dimensional density profiles of a hollow electron beam with the variations of (a) initial peak densities $n_{e0_{peak}} = 10^{15}$ (left), 5×10^{14} (center), and $2.5 \times 10^{14}\,\mathrm{m}^{-3}$ (right) for a fixed magnetic field intensity of 0.2 T and (b) applied magnetic field strengths $B = 0.1$ (left), 0.2 (center), and 0.4 T (right) for a fixed $n_{e0_{peak}} = 5 \times 10^{14}\,\mathrm{m}^{-3}$ at $t = 2.5 \times 10^{-7}$ s.

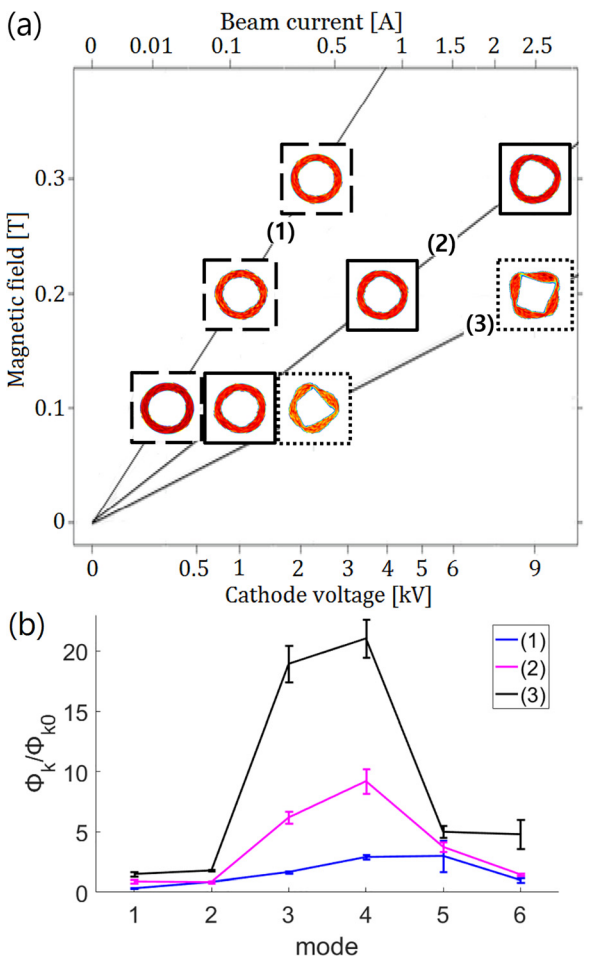

FIG. 5. (a) Density profiles and (b) normalized Fourier-transformed electrostatic potentials for the cases of uniform initial densities. The lines (1)–(3) indicate the cases with the scaling parameter $\sqrt{V[\mathrm{kV}]}/B[\mathrm{T}] = 5, 10, 15$, respectively.

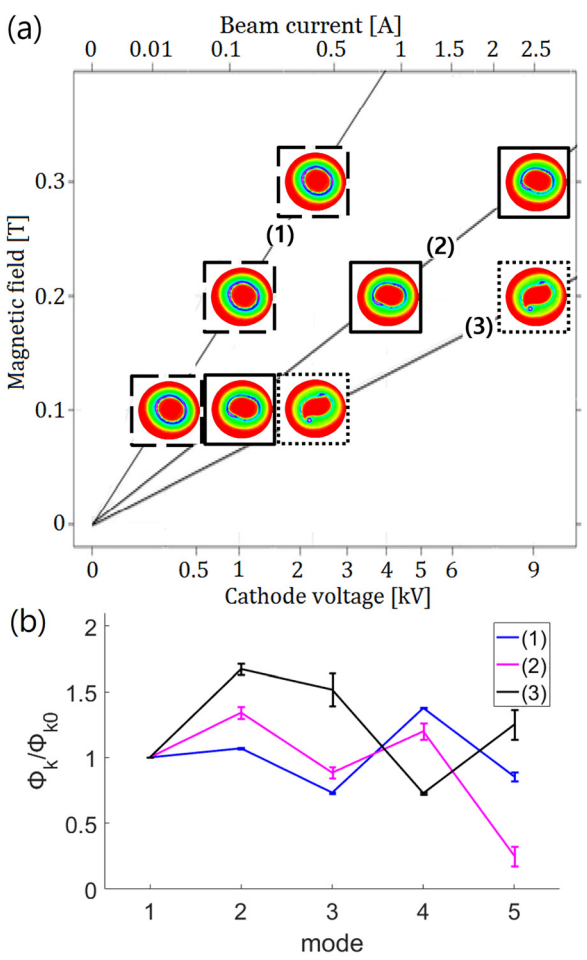

FIG. 6. (a) Density profiles and (b) normalized Fourier-transformed electrostatic potentials for the cases of non-uniform initial densities. The lines (1)–(3) indicate the cases with the scaling parameter $\sqrt{V[\mathrm{kV}]}/B[\mathrm{T}] = 5, 10, 15$, respectively.

same scaling parameter. All of these results indicate that the simulation results are in good agreement with the linear theory.

Figure 7 shows the comparison of numerical simulation with the experimental results.[20] Non-ideal conditions of the experiments, which are not considered in the simulations, cause some differences after propagating for a transit time ΔT. Nonetheless, we confirmed in both simulations and experiments that the scaling parameter $\sqrt{V}/B$ determines the degree of the beam cross-section evolution.

B. The effect of periodic dipole magnets

From now on, we investigate the effects of the periodic dipole magnets on the diocotron instability. Since an analytical solution for the evolution of the hollow electron beam with periodic dipole magnets is beyond the scope of this work, we discuss their possible effects through numerical simulations only. First of all, we note that the periodic dipole magnets, which are applied perpendicular to the propagation direction of the electron beam in addition to the solenoidal magnetic field along the propagation direction, can be considered as a temporally oscillating magnetic field in the beam frame of the two dimensional simulation. For the present simulations, the oscillating frequency of the magnetic field f_u is set in such a way that the magnetic field oscillates twice, while the beam passes through the propagation length once, i.e., $f_u = 2/\Delta T = 1.49 \times 10^7$ Hz. The reason for this parameter choice will be explained later. We will mainly focus on the effects of the different magnitudes of the dipole magnetic field for a fixed f_u.

The effects of the periodic dipole magnetic field are shown in Fig. 8. Simulations are performed with the conditions that the external magnetic field strength $B = 0.1$ T and the peak value of the electron density $n_{e0_{peak}} = 9 \times 10^{14}$ m^{-3} when there is no dipole magnetic field. Figure 8(a) clearly shows that the evolution of the diocotron instability slows down as B_u increases. It seems that the periodic dipole magnetic field impedes the rotation of the particles. For the analysis of the diocotron instability, the trajectories of only a few numbers of particles are plotted in Fig. 8(b) so that we can distinguish the differences in their velocity trajectories clearly. We expect that the velocity shear would be strong when the velocity differences between the particles at the outer and those at the inner sides are large. Figure 8(c) shows that the average azimuthal velocity v_Φ decreases with the increase in B_u. Hence, it appears that the stronger dipole magnetic fields are better for controlling the diocotron instability. However, due to the non-axial magnetic field components, we observe that the test particles drift back and forth in the radial direction as indicated in Fig. 8(b). This motion causes broadening of the density profile in the radial direction, which reduces the maximum density at the inner side of the hollow electron beam. While this density broadening does not affect the evolution of the diocotron instability so much, it is not desirable for the collimation of the proton beam. To keep the density at the inner side of the hollow electron beam high enough for the halo removal, therefore, we cannot increase the magnitude of the periodic dipole magnetic field too much. There is an optical value of B_u which is about 5 Gauss in the test case, with which the diocotron instability is mitigated while the beam broadening is not so large.

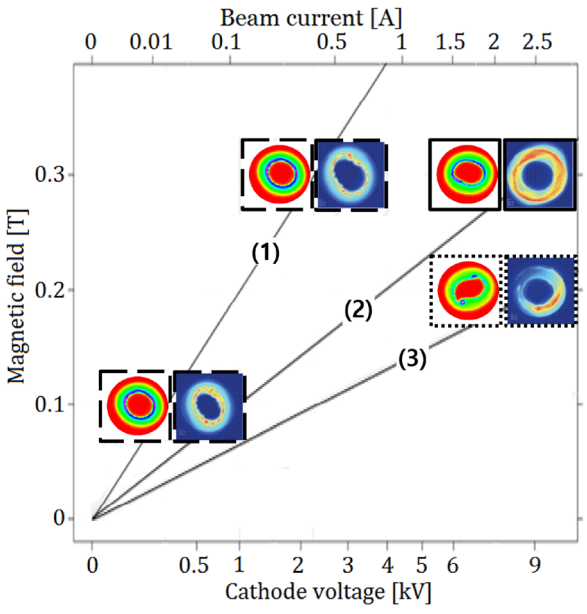

FIG. 7. Comparisons between numerical simulations and experimental results[20] for the cases of non-uniform initial densities.

Now, the reason why we choose the value of the oscillating frequency of the magnetic field to be $2/\Delta T$ can be explained in a similar manner. If the oscillating frequency of the applied magnetic field is too low, the particle motion in the radial direction is enhanced, and the density profile would be broadened. Thus, it seems obvious that a higher azimuthal frequency would be preferable in order to minimize the density broadening. However, there is also a problem for the high azimuthal frequency. When the frequency becomes too high, the particle motion becomes nearly similar to the case with only the axial magnetic field. In other words, the dipole magnetic fields would not have any stabilizing effects for the diocotron instability. Therefore, for the present study, we determined the value of f_u in such a way that the dipole magnetic fields provide a noticeable stabilizing effect for the diocotron instability while keeping the density broadening within an acceptable degree. We note that $f_u = 2/\Delta T$ corresponds to $m_\phi = 2$, which means that the magnetic field oscillates twice along the propagation length. Practically, this $m_\phi = 2$ magnetic field configuration could be easily implemented by an array of dipole magnets with a step-wise variation of the field strengths in the propagation direction of the beam.

VI. CONCLUSIONS

In this paper, the two-dimensional particle-in-cell simulations of the diocotron instability of a hollow electron beam are compared with the analytic theory and experimental observations. The relations between the diocotron instability and several physical parameters are reported, such as the electron density, the applied solenoidal magnetic field, and

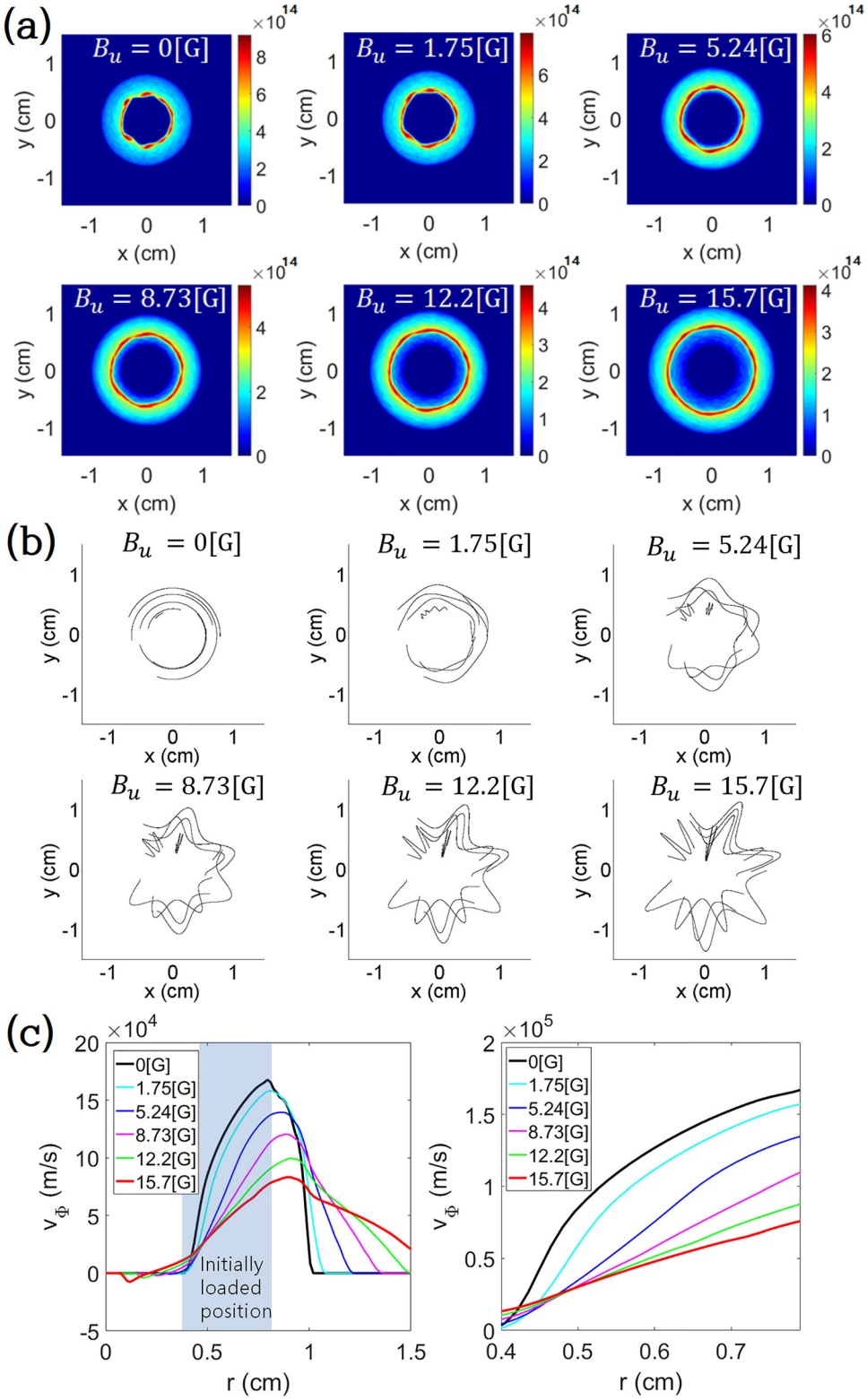

FIG. 8. (a) Density profiles, (b) traces of test particles, and (c) v_ϕ when the periodic dipole magnetic field is applied along the beam propagation with several different magnitudes at $t = 1.6 \times 10^{-7}$ s.

the acceleration voltage of the electron beam. The analytic growth rate is proportional to n/B theoretically, which can be expressed with a scaling parameter, $\sqrt{V}/B$ in experiments.

A method to control the diocotron instability of a hollow electron beam by applying periodic dipole magnetic fields has been investigated. It turns out that the method is effective for stabilizing the diocotron instability. More precisely, a stronger dipole magnetic field is better for stabilizing the diocotron instability but worse for collimating the proton beam because of the density broadening of the hollow electron beam. Therefore, an appropriate magnitude of the dipole magnetic field should be determined by considering a trade-

off between those two effects. We also note that the optimal periodicity of the dipole fields depends on the required electron beam density. In a practical application, where one may need to change beam current and transverse beam size, some flexibility on the periodic dipole field parameters may be required.

Since an analytical solution for the evolution of the hollow electron beam with periodic dipole magnets is beyond the scope of this work, we discussed their possible effects through numerical simulations only. A kinetic theory for the nonmodal shearing mode approach is a good tool to explain the instabilities in the sheared flow, which is our future work.

ACKNOWLEDGMENTS

This work was supported by the National R&D Program through the National Research Foundation of Korea (NRF) funded by the Ministry of Science, ICT & Future Planning (Grant No. NRF-2017R1A2B2011106), and by Fermilab operated by Fermi Research Alliance, LLC under Contract No. DE-AC02-07CH11359 with the U.S. Department of Energy. This work was partially supported by the U.S. DOE LHC Accelerator Research Program (LARP).

[1]R. C. Davidson, *An Introduction to the Physics of Nonneutral Plasmas* (Addison-Wesley, 2001).
[2]R. H. Levy, Phys. Fluids **8**, 1288 (1965).
[3]R. C. Davidson, H.-W. Chan, C. Chen, and S. Lund, Rev. Mod. Phys. **63**, 341 (1991).
[4]R. Davidson, Phys. Fluids **28**, 1937 (1985).
[5]J. H. Malmberg and J. S. deGrassie, Phys. Rev. Lett. **35**, 577 (1975).
[6]F. Driscoll, Phys. Rev. Lett. **64**, 645 (1990).
[7]G. Manfredi and P.-A. Hervieux, Phys. Rev. Lett. **109**, 255005 (2012).
[8]V. Shiltsev, in *Proceedings of the 3rd CARE-HHH-APD Workshop (LHC-LUMI-06)*, Valencia, Spain (2007), Paper No. CERN-2007-002, p. 92; in *Proceedings of the CARE-HHH-APD Workshop (BEAM07)*, Geneva, Switzerland (2008), Paper No. CERN-2008-005, p. 46.
[9]G. Stancari, A. Valishev, G. Annala, G. Kuznetsov, V. Shiltsev, D. A. Still, and L. G. Vorobiev, Phys. Rev. Lett. **107**, 084802 (2011).
[10]G. Stancari, V. Previtali, A. Valishev, R. Bruce, S. Redaelli, A. Rossi, and B. S. Ferrando, Fermilab Report No. TM-2572-APC (2014); e-print arXiv:1405.2033 [physics.acc-ph].
[11]S. Redaelli, A. Bertarelli, R. Bruce, D. Perini, A. Rossi, B. Salvachua, G. Stancari, and A. Valishev, in *Proceedings of IPAC* (2015), p. 2462.
[12]V. V. Mikhailenko, H. J. Lee, and V. S. Mikhailenko, Phys. Plasmas **19**, 082112 (2012).
[13]V. V. Mikhailenko, H. J. Lee, V. S. Mikhailenko, and N. A. Azarenkov, Phys. Plasmas **20**, 042101 (2013).
[14]V. V. Mikhailenko, J. S. Kim, Y. Jo, V. S. Mikhailenko, and H. J. Lee, Phys. Plasmas **21**, 052105 (2014).
[15]V. V. Mikhailenko, V. S. Mikhailenko, Y. Jo, and H. J. Lee, Phys. Plasmas **22**, 092125 (2015).
[16]Y. H. Jo, V. V. Mikhailenko, V. S. Mikhailenko, and H. J. Lee, J. Kor. Phys. Soc. **66**, 935 (2015).
[17]R. C. Davidson and G. M. Felice, Phys. Plasmas **5**, 3497 (1998).
[18]J. H. Booske, M. A. Basten, and A. H. Kumbasar, Phys. Plasmas **1**, 1714 (1994).
[19]J. P. Verboncoeur, M. V. Alves, V. Vahedi, and C. K. Birdsall, J. Comput. Phys. **104**, 321 (1993).
[20]V. Moens, Master's thesis, Ecole Polytechnique, Lausanne, Switzerland, 2013.